



Performance analysis for the CALIFA Barrel calorimeter of the R³B experiment



H. Alvarez-Pol^{a,*}, N. Ashwood^b, T. Aumann^{c,d}, D. Bertini^d, P. Cabanelas^a, E. Casarejos^e, J. Cederkall^f, D. Cortina-Gil^a, P. Díaz Fernández^a, I. Duran^a, E. Fiori^{g,h}, D. Galavizⁱ, M. Labiche^j, E. Nacher^k, B. Pietras^a, D. Savran^{g,h}, O. Tengblad^k, P. Teubigⁱ

^a Dpt. de Física de Partículas, Universidade de Santiago de Compostela, E-15782, Santiago de Compostela, Spain

^b School of Physics and Astronomy, University of Birmingham, Edgbaston, Birmingham B15 2TT, United Kingdom

^c Institut für Kernphysik, Technische Universität Darmstadt, D-64289 Darmstadt, Germany

^d GSI Helmholtzzentrum für Schwerionenforschung GmbH, D-64291 Darmstadt, Germany

^e Universidade de Vigo, E-36310 Vigo, Spain

^f Department of Physics, Lund University, SE 221 00 Lund, Sweden

^g ExtreMe Matter Institute EMMI and Research Division, GSI Helmholtzzentrum für Schwerionenforschung GmbH, D-64291 Darmstadt, Germany

^h Frankfurt Institute for Advanced Studies, D-60438 Frankfurt am Main, Germany

ⁱ Centro de Física Nuclear da Universidade de Lisboa, 1649-003 Lisbon, Portugal

^j STFC Daresbury Laboratory, Warrington WA4 4AD, United Kingdom

^k Instituto de Estructura de la Materia CSIC, Madrid, Spain

ARTICLE INFO

Article history:

Received 15 April 2014

Received in revised form

9 July 2014

Accepted 8 September 2014

Available online 19 September 2014

Keywords:

Calorimetry

Simulation

Gamma detection

Proton detection

Exotic beams

Fast beams

ABSTRACT

The CALIFA calorimeter is an advanced detector for gamma rays and light charged particles, accordingly optimized for the demanding requirements of the physics programme proposed for the R³B facility at FAIR. The multipurpose character of CALIFA is required to fulfil challenging demands in energy resolution (5–6% at 1 MeV for gamma rays) and efficiency. Charged particles, e.g. protons of energies up to 320 MeV in the Barrel section, should also be identified with an energy resolution better to 1%.

CALIFA is divided into two well-separated sections: a “Forward EndCap” and a cylindrical “Barrel” covering an angular range from 43.2° to 140.3°. The Barrel section, based on long CsI(Tl) pyramidal frustum crystals coupled to large area avalanche photodiodes (LAAPDs), attains the requested high efficiency for calorimetric purposes. The construction of the CALIFA Demonstrator, comprising 20% of the total detector, has already been initiated, and commissioning experiments are expected for 2014.

The assessment of the capabilities and expected performance of the detector elements is a crucial step in their design, along with the prototypes evaluation. For this purpose, the Barrel geometry has been carefully implemented in the simulation package R3BRoot, including easily variable thicknesses of crystal wrapping and carbon fibre supports. A complete characterization of the calorimeter response (including efficiency, resolution, evaluation of energy and reconstruction losses) under different working conditions, with several physics cases selected to probe the detector performance over a wide range of applications, has been undertaken. Prototypes of different sections of the CALIFA Barrel have been modeled and their responses have been evaluated and compared with the experimental results. The present paper summarizes the outcome of the simulation campaign for the entire Barrel section and for the corresponding prototypes tested at different European installations.

© 2014 Elsevier B.V. All rights reserved.

1. Introduction

With the advent of the new facility FAIR [1], a constellation of reaction experiments at relativistic energies, exploring the most exotic

nuclei ever identified, opens for the NuSTAR (NUclear STructure, Astrophysics and Reactions) community [2]. At these energies, the use of thick targets and a large solid angle coverage of the outgoing particles allow the study of the participants' structure and the underlying reaction mechanisms over a wide range of reaction channels.

The R³B [3] (Reactions with Relativistic Radioactive Beams) experiment at FAIR will provide the capability for kinematically complete measurements of reactions with relativistic beams of

* Corresponding author.

E-mail address: hector.alvarez@usc.es (H. Alvarez-Pol).

exotic nuclei far from stability, up to around 1 A GeV. The experimental setup currently under construction has been designed by the international R³B collaboration based on more than 20 years of experience with the LAND/ALADIN reaction setup, overcoming its limitations and improving the global performances. It will provide sufficiently high resolution to enable a comprehensive experimental investigation of fundamental questions relating to nuclear structure, astrophysics, and reactions with extreme isospin-asymmetric nuclei.

One of the key detectors in the R³B setup is the CALIFA calorimeter (CALorimeter for the In Flight detection of gamma rays and light charged pArticles) that will surround the reaction target. It will serve as a high-resolution gamma ray spectrometer as well as a high efficiency calorimeter, identifying high-energy charged particles simultaneously. This multipurpose character is an essential functionality for the success of the broad experimental programme of R³B. The CALIFA detector is divided into two separate sections: a “Forward EndCap” for forward polar angles below 43° and a cylindrical “Barrel” covering an angular range from 43.2° to 140.3°.

The present work studies the response of the Barrel to gamma and proton detection, in terms of its efficiency, energy resolution, the evaluation of the impact of the passive matter in the detector and the ability to extract the underlying reaction properties under different working conditions, including several selected physics cases of interest for the R³B program. Section 2 contains a description of the CALIFA Barrel characteristics and specifications. In Section 3 the tools for the simulation and event reconstruction are thoroughly described. The simulated response is described in Sections 4 and 5 for gammas and protons, respectively. Finally, a simulation set of selected physical cases has been analyzed in Section 6, before the section Summary and conclusions.

2. Description of the CALIFA barrel

The detection units of the Barrel part of the CALIFA detector are made of long CsI(Tl) pyramidal frustum crystals with a rectangular base, coupled to large area avalanche photodiodes (Hamamatsu S12102 LAAPD, with two 10 × 10 mm² sensors) [4]. The particular design of the detector has been developed to fulfill the challenging demands for energy resolution and efficiency, the requirements are detailed in Table 1. The fast projectile kinematics suffer a large Lorentz broadening; even if the energy were perfectly determined, a limited polar angle resolution would contribute to the uncertainty after the Doppler correction. The chosen granularity is a trade-off between energy resolution and Doppler broadening [5,6].

Charged particles, e.g. protons of energies up to 320 MeV, should be identified with an energy resolution better to 1%. Both features can be satisfied simultaneously by a careful design based on carbon fibre alveolar support structures with a minimum of interposed matter [7] (see Fig. 1). The crystals are shaped according to the required granularity, focusing on the reduction of empty space and passive materials, to minimize the gamma ray fraction escaping through spaces

Table 1

Nominal specifications of the CALIFA calorimeter (valid for incoming fragments with $\beta=0.82$). These parameters are defined by the physics program outlined in the R³B Technical Proposal [3]. Δ stands for energy resolution measured in terms of FWHM.

Intrinsic photopeak efficiency	40% (at $E_\gamma=15$ MeV projectile frame)
γ Sum energy resolution $\Delta(E_{sum})/E_{sum}$	< 10% for 5 γ rays of 3 MeV
γ Energy resolution	5–6% $\Delta E/E$ for 1 MeV γ rays
Calorimeter for high energy light charged particles (LCP)	Up to 320 MeV in lab. system
LCP energy resolution	$\Delta E_p/E_p < 1\%$
Proton- γ separation	For 1–30 MeV

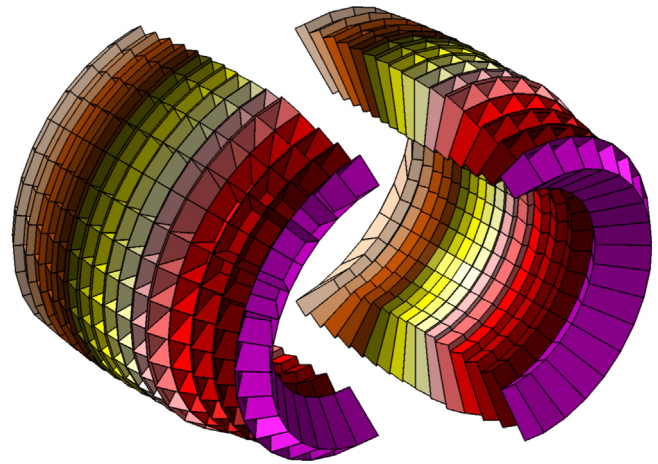


Fig. 1. Artistic view of the Barrel carbon fibre structure containing the crystals.

among the active bulk. A reduced set of different crystals was selected. The length of the crystals is determined according to the detection efficiency required at the energy corresponding to each angular region, matching the expected gamma energy modification driven by the Lorentz boost. The selection of the scintillator material and the photo-sensors is the result of a long R&D period investigating the optimization of the wavelength and the optical matching, light transmission, wrapping materials and the associated electronics response [4,8–11].

The Barrel is composed of 1952 crystals in six different geometries. Crystals are arranged in the carbon fibre alveoli in sets of four, each set consisting of two chiral pairs. The last alveolus type, covering the most backward angles, is filled with a single crystal. The inner radius is around 30 cm, with an approximate crystal volume and weight of 285 l and 1300 kg, respectively.

Several prototypes have been constructed and tested to probe the competence of the concept to reach the required specifications, each corresponding to different kinematical regions of the CALIFA detector [12]. The construction of the CALIFA Demonstrator, which comprises 20% of the total detector, has already been initiated, and commissioning experiments are expected for 2014. A particular effort has been devoted to the development and analysis of simulations driving the design of the calorimeter. The unprecedented requirements for proton and particle detection performance necessitated a dedicated simulation study accompanying an in-depth investigation encompassing the major modern developments in detector technology.

3. The Barrel implementation in the R3BRoot code

The reconstruction capabilities of the CALIFA detector may be obtained from the thorough analysis of a complete and detailed simulation. Event generators establish the initial point for the simulation of the physical cases of interest, as well as providing the source of different particles for the evaluation of the detector. These particles are tracked in the setup, interacting with the matter and depositing some energy in the sensitive volume of the detectors, which has to be properly reconstructed according to the individual crystal characteristics.

The R3BRoot code [13,14] is an instance of the FAIRRoot framework developed for the description, simulation and data analysis of the R³B setup and experiments. The FAIRRoot framework [15] is based on the ROOT [16] code. The user can create simulated data and perform analysis within the same framework. Moreover, Geant3 and Geant4 [17] transport engines are supported; however, the user code that creates simulated data does not depend on a particular Monte Carlo engine. The framework delivers base classes which enable the

users to construct their detectors and analysis tasks in a simple way. The R3BRoot code derives from the general classes of FAIRRoot, adding and specifying the geometrical, physical description and response of the detectors of the R³B setup, magnetic field maps, event generators for the reactions of interest and analysis and event visualization tools. It expands the framework behavior by including a dedicated physics list for low energy neutrons, gamma interactions and nuclear fragment transport while supporting database connectivity to handle multiple experimental setups.

The CALIFA Barrel is comprehensively detailed inside the R3BRoot simulation and data analysis code. The geometrical description of the CALIFA detector includes the CsI(Tl) crystals corresponding to precise manufacturing specifications, the wrapping of the crystals with a variable thickness parameter for probing their influence on the event reconstruction and the carbon fibre alveoli that provide a support structure for the crystals, also with variable thickness. Additionally, most of the relevant elements or detectors relating to the passage of matter between the production vertex and the calorimeter elements are defined, including a vacuum chamber, the inner silicon tracker detectors and the reaction target.

The energy deposited per event in each crystal by all interacting particles is added and stored. The response of the detector is expected to be proportional to the total energy deposited. Effects exist that cause a deviation from this behavior, such as non-linearity in the light output-energy correlation and the light output non-uniformity (LONU) due to the dependence on the gamma ray interaction position. This last effect has been taken into account by introducing a variable, step-like function, smearing the detector response.

Two different data structures have been developed to account for the expected response of the crystals and the calorimeter. First, for each crystal where energy has been deposited, a *Crystal Hit* structure is filled, containing the total energy, the time of the first interaction in the crystal and the crystal identifier. Second, as a result of the analysis of the event topology, a second data structure named *Calorimeter Hit* is filled containing the “clusters” or groups of *Crystal Hits* which are expected to correspond to the same nuclear emission.

The presence of the EndCap detector influences significantly the evaluation of the response of the Barrel detector. First, it should be included for the physical cases where the reconstruction requires a detector for forwardly emitted light charged particles, as for the case of the quasi-free scattering (QFS). Second, even in those cases where it is not essential for the reconstruction, as for spectroscopic studies, it represents a considerable source of radiation scattering to be detected in the Barrel part and a detection element for part of the radiation that escapes from the Barrel in the forward direction. Presently as the final design is still far from completion, a preliminary version of a EndCap candidate detector based on similar construction principles to the Barrel was included in the simulations.

3.1. Event generators

The evaluation of the performance of the CALIFA Barrel under different physics scenarios requires the construction of appropriate event generators. Several event generators have been developed, ranging from trivial gamma ray and particle distributions for testing the characteristics of the detector, to complex experimental events, to evaluate the reconstruction capabilities.

A flexible code producing distributions of gammas or charged particles is integrated within the R3BRoot event generators. The generator allows the selection of the particle type, angular emission (both in polar and azimuthal angles or angular region), the momentum (or momentum range), multiplicity and position of the emitted particles. Additional functions allow the generation of a flat distribution on the cosine of the polar angle for an isotropic

angular emission, the random location of the vertex inside a volume which simulates an interaction within the target and the addition of the Lorentz boost for gammas, with selectable projectile velocity. This trivial generator has been used for the study of the core characteristics of the CALIFA Barrel described in this work.

For nuclear spectroscopy and the study of Giant and Pygmy resonances, a gamma cascade generator has been built. The input for the generator is an ASCII text file in which the user can set the speed of the projectile (β , for generating the Lorentz boost), its uncertainty due to the thickness of the target, and the main characteristics of the de-excitation pattern. The latter includes the position of a Giant Dipole Resonance (GDR), a Pygmy Dipole Resonance (PDR) if applicable, their respective widths, the probability to populate each of the resonances in the reaction, the position of all the spectroscopic levels, the probability to populate each level in the reaction, and finally, a branching ratio matrix which connects all the different levels and the resonances.

Fig. 2 shows an example of level scheme, branching ratios and population distribution that one might generate. The level at 9.5 MeV is a broad resonance as one can see in the left spectrum (population) of the figure.

The output of the event generator, which is in fact the input for the simulation, can be seen in Fig. 3. In the left pad, the gamma ray spectrum in the projectile frame (PF) is shown. These gammas are emitted isotropically in the PF frame. The right pad represents the same gamma ray spectrum once the Lorentz boost is applied ($\beta=0.5$ in this case), therefore in the Laboratory frame (Lab). In the laboratory frame each energy peak is spread between a minimum and a maximum energy which depends on the emission angle and the projectile velocity. The emission of the gamma rays in the Lab frame is not isotropic anymore but focused forward by the Lorentz boost. In the particular case shown here, gamma cascades of multiplicity up to five have been generated.

The gamma cascade generator can be used to generate events with low multiplicity and low energy gamma rays instead of GDR examples, simply by setting the probability to populate the resonance equal to zero and defining a simple level scheme containing a few low energy levels.

Other event generators are available for specific reactions of interest. In particular, a kinematical quasi-free scattering (QFS) code based upon the Goldhaber model [18], where the energy of the projectile nucleus is shared between the scattered protons in a way that is determined by their scattering angle, and hence the binding energy or internal momentum of the proton removed from the nucleus. The QFS $^{12}\text{C}(p,2p)^{11}\text{B}$ has been studied in this

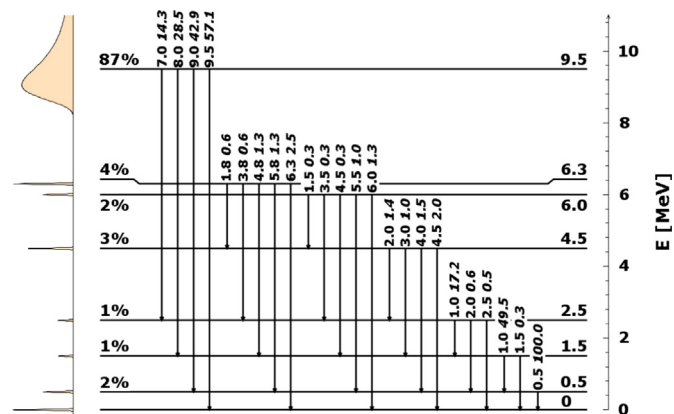


Fig. 2. Example of a generated decay scheme of a Giant Dipole Resonance. The energy, in MeV, is written on the right side of each level while the population probability, in percent, on the left side and in the left graph. For the transitions, the energy and the branching ratio in italics (normalized to the strongest transition) are shown.

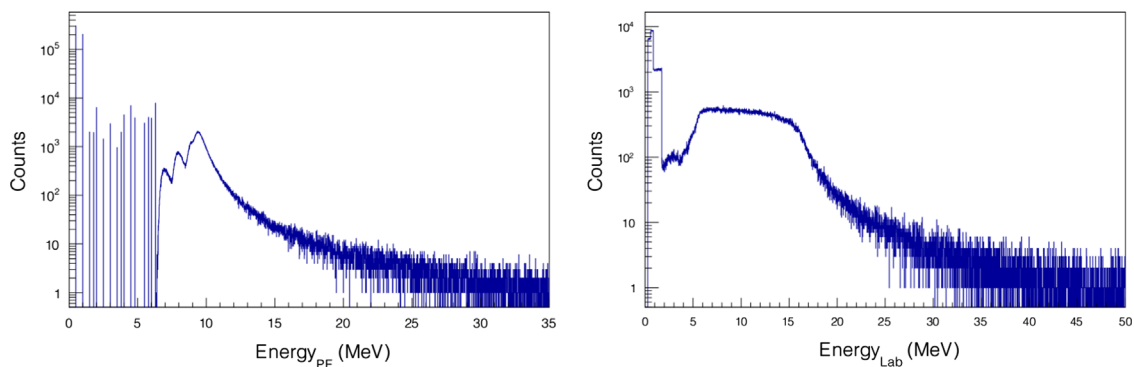


Fig. 3. Left: gamma ray energy spectrum in the projectile frame (PF), corresponding to the decay represented in Fig. 2. Right: the same gamma ray energy spectrum but in the laboratory frame, where all the individual peaks smeared due to the Lorentz boost.

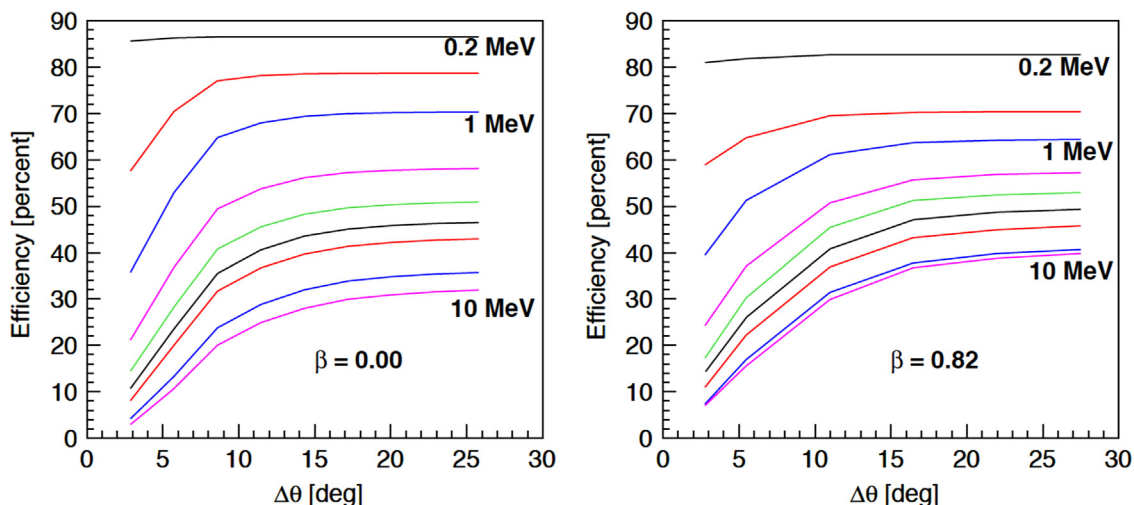


Fig. 4. Dependence of the efficiency of the clustering algorithm on the solid angle for add-back (circular window) for various energies (from top to bottom: 0.2, 0.5, 1, 2, 3, 4, 5, 8 and 10 MeV) and multiplicity one. Left: the source emitting the photons was at rest, i.e. $\beta=0$. Right: the velocity of the source was set to $\beta=0.82$.

way, merging the proton distributions with Lorentz boosted gamma ray events emitted from the ^{11}B excited states decay.

3.2. Event reconstruction

Depending on the reaction under study, one or more particles are expected to be detected simultaneously by CALIFA. In addition, low-energy background produced via bremsstrahlung in the target or other reaction mechanisms will contaminate the energy spectra. Thus, the development of intelligent reconstruction algorithms for both gamma rays and protons becomes mandatory in order to maximize the detection efficiency and resolution and optimize the individual reconstruction of the incident particles and the identification of possible contributions in the low-energy background dominated region.

The most basic approach consists of summing up (add back) the energy of all the crystals in a selected angular region. Two different options were adopted when considering the angular region for add-back purposes: a circular window, with just one parameter $\Delta\theta$ defining the solid angle covered by the window; and a square one in the space defined by the two parameters $\Delta\theta$ and $\Delta\phi$, the polar and azimuthal angles. The crystal hit with the maximum energy in each event is chosen as the first cluster centre. All hits falling into the angular region around this centre, as defined by either of the two approaches, are assigned to the cluster. Next, the crystal with the highest energy not included in the previous cluster is chosen as

the next cluster centre, and the procedure is repeated until all hits above the detection threshold have been assigned to a cluster. The incoming angle is assigned by the angle of the cluster centre. The performances of the two different definitions for the angular window were found to produce very similar results.

Simulations were performed considering photons of several energies (ranging from 0.1 to 10 MeV in the rest frame of their emitter) under conditions equivalent to those expected in R^3B , emitted from a source at rest or moving at a velocity $\beta=0.82$. The emission angles were distributed isotropically within the Barrel solid angle. For a single gamma ray per event, of energy E_γ , the efficiency corresponds to the number of entries under the photopeak normalized to the total number of gamma rays emitted into the solid angle covered by the Barrel. Thus, the calculated efficiency considers the intrinsic efficiency of the barrel, but does not include the geometric acceptance.

In order to evaluate the performance of the reconstruction algorithms, the angular window parameters were varied, analyzing the cases of a source at rest and moving at $\beta=0.82$. The results of simulations with multiplicity one are shown in Fig. 4, where the obtained photopeak efficiency is presented as a function of the angular parameter at several energies.

From both figures we observe that, independent of the velocity of the source emitting the gamma rays, there is a certain angular window for which the algorithm saturates. This angular region shows a clear dependence on the energy of the photons, implying that the angular window should take into account the amount of

energy detected. The implementation of the energy dependence of the angular reconstruction parameter is an on-going work, which will improve the overall efficiency of the algorithm.

The shape of the efficiency curve for a given photon energy has been also studied for various multiplicities. Fig. 5 presents the photopeak efficiency for gamma rays of 1 MeV with multiplicities ranging from 1 to 7. In this way, the effect of the decrease of photopeak efficiency due to intermixing of hits stemming from different photons becomes evident and is directly represented by the loss of efficiency for higher multiplicities. The saturation effect observed for multiplicity one is due to the reaching of the maximum spread of the interactions in the scintillating material. For higher multiplicities this effect is combined with the mixing of crystal hits stemming from separate gamma rays which leads to an erroneous determination of the initial gamma ray energy.

The performed studies also show the limited capability of this simple reconstruction algorithm. Thus, ongoing work focuses on the development of additional methods that would improve the performance of CALIFA in the reconstruction of the correct energy when more than one photon enters the detector. A promising option for photon recovery lies in the use of artificial neural networks (ANN) [19]. For each event, the ANN takes a number of parameters to best select the method for event reconstruction. Such parameters could include the crystal-fold distribution, the maximum energy recorded by a single crystal, the total energy, the angle of the gamma rays and the probability of interaction type within the crystal. The refinement of this method is reliant upon the R3BRoot simulation framework, while rigorous experimental verification of ANN methods will be possible with the aforementioned CALIFA Demonstrator. Development is ongoing (but not used in this paper) and should provide a highly flexible and sophisticated method for reconstruction [20].

4. Response to gamma rays

Within this section, the response of the CALIFA Barrel to gamma rays emitted from a fast projectile will be explored. The R3BRoot analysis framework interfaces with the Geant4 tracking engine, using electromagnetic standard physics: all the inner detectors and support structures were defined, including a plastic target (CH_2) of 1 cm radius and 0.1 cm thickness, the multilayer silicon tracker detector and the reaction chamber. Gammas have been emitted isotropically from a cubic box with ± 2 mm length for each axis around the origin, located in the centre of the target volume. A Lorentz boost with $\beta=0.82$, corresponding to a projectile energy of

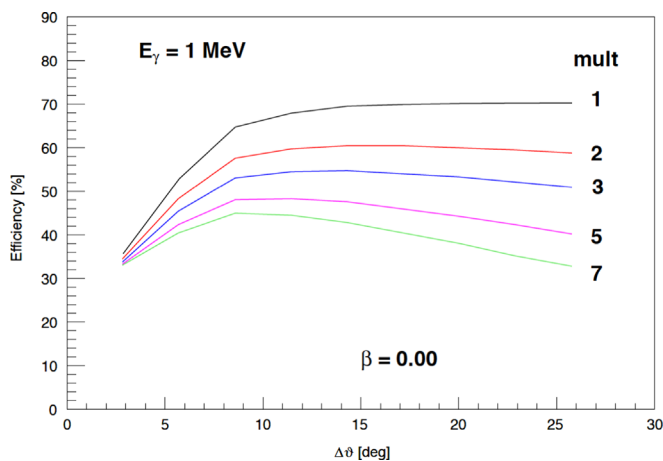


Fig. 5. Efficiency versus cluster window size for different multiplicities of the simulated event (from top to bottom: multiplicity 1, 2, 3, 5, 7) and a gamma ray energy of 1 MeV.

700 A MeV, has been applied to the emitted gamma rays. As a result, the laboratory energy distribution is flat, varying between approximately 0.4 and 3 times the original energy, the angular distribution peaking at a polar angle of approximately 20° .

The crystal intrinsic non-uniformity has been included by simulating a 1% maximum random deviation from the original energy deposited in the scintillator material. A Gaussian smearing of 4%, 5% and 6% at the energy of 1 MeV, scaling with the square root of the energy, has been used to represent the experimental resolution. "Perfect" detectors, with no energy smearing, have been additionally simulated to represent the geometrical contribution to the total resolution.

The reconstruction algorithm with an optimized "square window" of $\sim 15^\circ$, described in the previous section, provides the candidate gamma rays from the clusters. The cluster crystals energy deposition is summed if exceeding an energy threshold. The stability of the results has been tested against different values of the energy threshold, namely 20, 50 and 100 keV; a value of 50 keV has been used in the results here included. The polar angle, needed for the Doppler correction, is taken from the centres of both the target and the crystal with largest energy in the cluster.

The CALIFA Barrel and the complete calorimeter have been tested using gamma rays emitted with energies between 200 keV and 15 MeV in the projectile frame. The upper pad of Fig. 6 shows the dependence on the gamma energy in the projectile frame of the

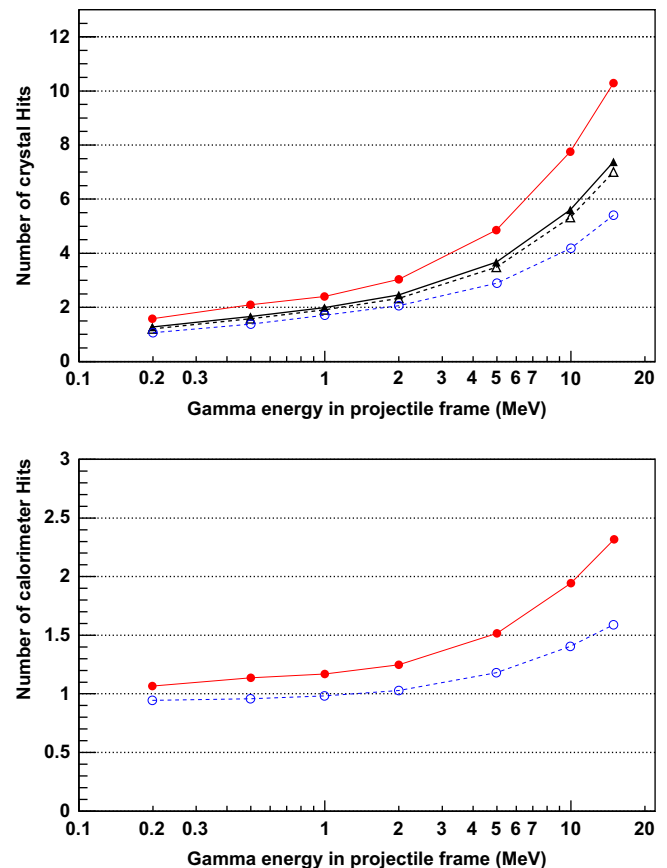


Fig. 6. Upper pad: mean number of crystals with signal vs. the emitted gamma rays energy, in the projectile frame (moving at $\beta=0.82$). Results are displayed separately for the Barrel (open circles over the dashed line) and the EndCap (solid circles over the solid line), while those in between are obtained for the complete CALIFA, and normalized with respect to the total number of emitted gamma rays (open triangles over dashed line) or the total number in the calorimeter geometrical aperture (filled triangles and line). Lower pad: dependence of the mean number of clusters with the emitted gamma ray energy in projectile frame in Barrel (open circles over the dashed line) and EndCap (solid circles and line) regions.

mean number of crystals with signal above threshold for the separate Barrel (open circles over the dashed line) and EndCap (filled circles) sections. This number is obtained by dividing the number of crystals with signal above threshold by the total number of emitted gamma rays in the geometrical acceptance of each detector section. In between, the mean number of crystals for the whole calorimeter is quoted, normalized to the total number of emitted gamma rays (open triangles) or to the total number of gamma rays only in the calorimeter geometrical aperture (filled triangles). The lower pad shows the number of clusters (or *Calorimeter Hits*) obtained when the reconstruction algorithm is applied, separately for the Barrel (open circles over the dashed line) and EndCap (solid circles and line) regions. Here, the total number of reconstructed clusters is divided by the total number of emitted gamma rays in the geometrical acceptance of each element.

The number of crystal hits (or crystal-fold) is only around one for the lower energies studied. At energies around 1 MeV, the mean number of crystal hits is already above two, the crystal-fold in the EndCap region being much larger than in the Barrel, due to the characteristics of the Lorentz boost. The mean number of crystal hits increases at high energy, reaching values above 4 for projectile frame energies of 10 MeV in the Barrel region, and close to 8 in the EndCap volume. Nevertheless, the crystal-fold distribution is quite broad, with around 10% of 1 MeV gammas depositing energy over three or more crystals in the Barrel, while in the detection of gammas at 10 MeV, events with crystal-fold above 10 are still quite probable (close to 1% of the cases for the Barrel).

The lower pad of Fig. 6 displays the dependence of the mean number of clusters (*Calorimeter Hits*) with the emitted gamma ray energy in the projectile frame. The mean cluster-fold is around one at low energy. This number is slightly below one for the Barrel, due to the inefficiency factors (gamma rays lost in the inactive volume or stopped in the matter before the active volume). At high energy, the mean cluster-fold is well above one, indicating that the algorithm with a single window is not able to collect in a unique cluster all the crystals with signal. These crystals could be located over quite a distance due to the predominant interaction processes (Compton and pair production). As in the case of the crystal hits, the lower pad of Fig. 6 displays mean values. The complete cluster-fold distribution shows a non-negligible probability of two clusters at low energy and, for the highest energy tested, 5% of the gamma rays produce more than five clusters.

4.1. Energy resolution

The energy resolution is one of the most relevant parameters to evaluate the capabilities of CALIFA to perform the R³B Physics program. To a large extent, the energy resolution is given by the scintillator and the readout properties. However, the particular characteristics of the gamma ray kinematics make calorimeter design and granularity important elements in the energy resolution assessment.

The energy resolution is defined as

$$R = \frac{\text{FWHM}}{E_\gamma} = \frac{2\sqrt{2 \ln 2} \sigma}{E_\gamma} \approx \frac{2.355 \sigma}{E_\gamma} \quad (1)$$

where σ and E_γ are obtained from the Gaussian fit to the photopeak. This definition works correctly at low and intermediate energy, but at higher energies there is a deviation of the gamma ray full energy peak reconstruction from the Gaussian shape, with the emergence of a low energy tail on the peak.

The top pad of Fig. 7 shows the dependence of the resolution with the emitted gamma ray energy in the projectile frame for the full calorimeter. The different curves (solid lines and circles) correspond to different values of the crystals energy resolution: from the top to the bottom results for an experimental intrinsic resolution of 6, 5 and 4% and 4%

at 1 MeV (scaling with the square root of the energy) are displayed, while the lower curve (open markers) corresponds to ideal detectors, where the sole contribution to the resolution is the Lorentz broadening. The additional set of square markers (dashed lines) represents the case where a sum over all crystals was employed. They differ only at high energy, 5 MeV and above, where the resolution is better when all the crystals energy is added. This difference is another indication that, for the most energetic gamma rays, part of the energy could escape to large distances from the initial interaction point, complicating the reconstruction of clusters. Selecting a larger angular window would include this portion of the energy, conversely decreasing the efficiency for events with larger multiplicity.

At low energies, the energy resolution is dominated by the intrinsic crystal resolution. At larger energies, above 2 MeV in the projectile frame, the granularity of the detector dominates, with the Lorentz broadening becoming the larger contribution to the energy resolution as the energy increases. It is worth noting that the granularity has been chosen to reduce the geometrical contribution to the energy resolution to approximately 4%.

It is important to remember that the energies quoted in the abscissa in Fig. 7 (and others in this section) correspond to energy emitted in the projectile frame. In the laboratory frame, a single energy value transforms into a value from 0.7 to 3 times the projectile frame energy over the range of the polar angles covered by the Calorimeter. The laboratory frame energies at the Barrel region being smaller than in the EndCap, resulting in a different set of curves for the efficiency and the resolution (see the lower pad of

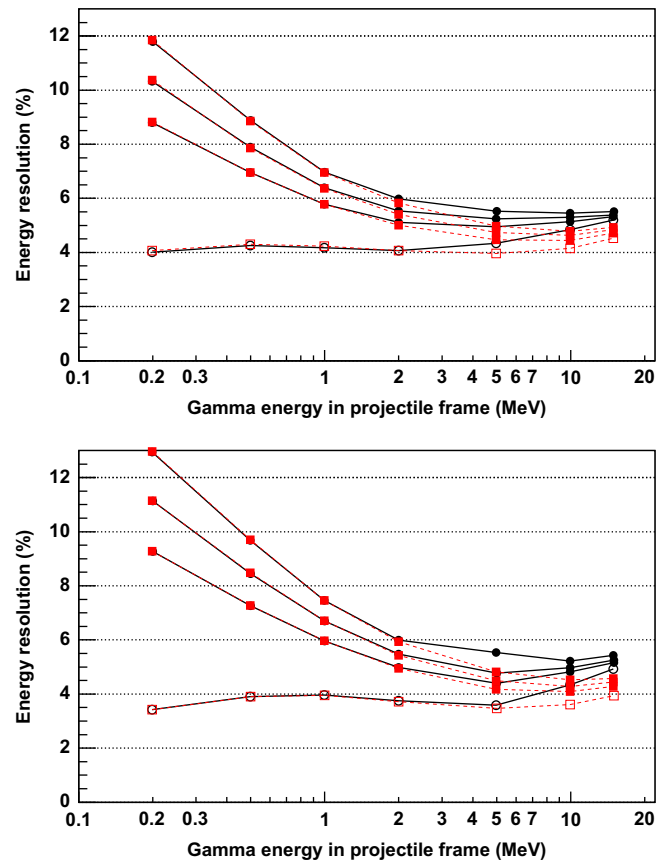


Fig. 7. Upper pad: full calorimeter dependence of the resolution with the emitted gamma ray energy in the projectile frame. From the top to the bottom, in solid circles and lines, results for intrinsic resolution of 6, 5 and 4% at 1 MeV (scaling with the square root of the energy) are displayed. The lower curve (open markers) corresponds to ideal detectors. The squares represent the same set of curves with add-back in all the calorimeter crystals. Lower pad: dependence of the resolution with the emitted gamma ray energy in projectile frame for the Barrel. The meaning of the different markers is the same as for the top pad. In both cases $\beta=0.82$.

Fig. 7). Only gamma rays entering in the geometrical acceptance of the Barrel have been considered for the evaluation of the Barrel properties. The meaning of the different curves and markers corresponds to that in the top pad. The resolution at low energy is slightly worse than in the full setup, while at large energies the resolution improves slightly. Both effects are caused by the Lorentz boost in the polar angles covered by the Barrel; as these angles are larger, the gamma ray energies are lower, decreasing even from the original energy in the projectile frame.

4.2. Efficiency

The efficiency of the CALIFA Barrel has been one of its key requirements and a huge effort has been dedicated to improve this feature in the calorimeter concept and design. This subsection involves a detailed evaluation of the results for the detection of a single gamma ray and also for events of multiplicity 3. The photopeak or full absorption efficiency is the key parameter in this evaluation. It is defined as the ratio between the number of gamma rays which are reconstructed with their complete energy and the total number of emitted gamma rays. The definition depends on what “complete energy reconstruction” is considered. In this section, the energies included within a window in the interval $[-2\sigma, 2\sigma]$ of the Gaussian function fit of the photopeak have been taken. This criterion is quite conservative at low energies, discarding entries in the tails of the peak which could be considered as well reconstructed. But it is useful to avoid the inclusion of reconstructed gamma energies in the left part of the photopeak for the largest energies, where the photopeak shape deviates from a Gaussian distribution.

The top pad of Fig. 8 represents the photopeak efficiency for the entire calorimeter. The photopeak efficiency could be normalized to the total number of emitted gamma rays, independently of their direction (geometrically uncorrected) or to the number of gamma rays that are emitted in the geometrical acceptance of the part of the detector under consideration (geometrically corrected). The data shown in the figure correspond to the latter definition. The difference between the two cases amounts to $\sim 5\%$, due to undetected particles directed to regions not covered by the calorimeter elements (beam line pipe, backward angles aperture).

The two data sets shown in the top pad of Fig. 8 correspond to the results for different settings of the angular window in the reconstruction algorithm: a sum over all crystals in the case of the triangular markers, and the optimized angular window represented by stars (around 15°). At low energy both algorithm parameters return a similar result, while in the mid-high energy region, above projectile frame energies of 1 MeV, the efficiency drops by around 10% when the add-back is limited to a set of crystals and not to the full calorimeter, indicating that part of the energy is deposited in crystals which could be quite far away, as it was previously concluded from the study of the mean number of clusters.

Efficiency at low energies varies between 70 and 80%, and is continuously dropping at larger energies. It is worth mentioning that at the largest gamma ray energies tested, the total calorimeter efficiency still remains quite high (around 40% at 15 MeV). Direct comparison with other devices is complex: CALIFA has been designed for the particular kinematics of the particle emission from fast projectiles at approximately the velocity of the beam. The capability to correct for the Doppler broadening makes CALIFA a unique instrument for the analysis of particles emitted in reactions at these energies.

The efficiency of the Barrel section is shown in the lower pad of Fig. 8. Here, both the geometrical acceptance uncorrected (circle markers) and corrected (square markers) photopeak efficiencies are shown; the first curve indicates the efficiency combining intrinsic and

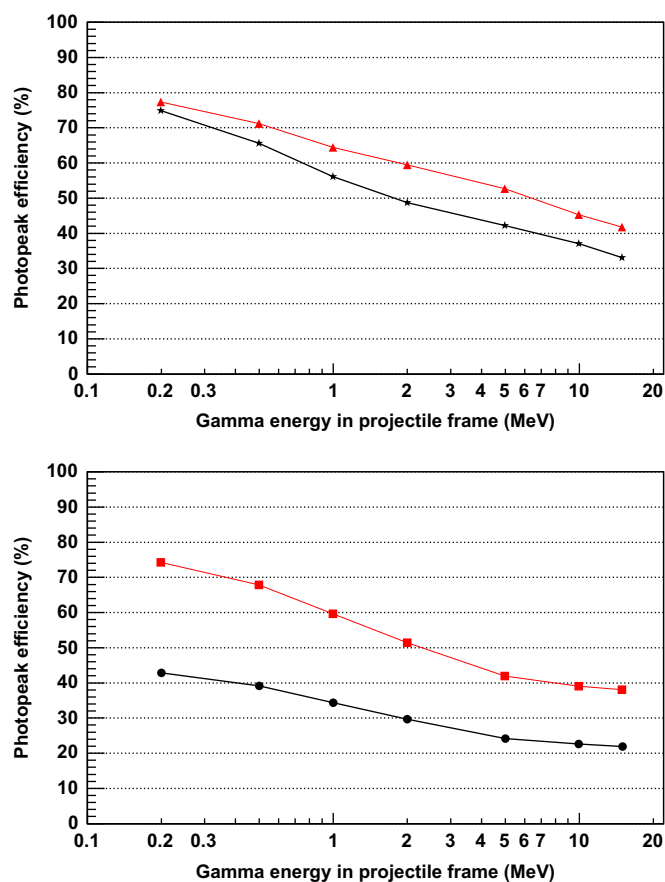


Fig. 8. Upper pad: dependence of the photopeak efficiency with the emitted projectile frame gamma ray energy for the entire calorimeter. The star markers represent the results for an optimized angular window in the reconstruction algorithm, while triangular markers stand for the sum of the energy in all crystals. Lower pad: dependence of the photopeak efficiency with the emitted projectile frame gamma ray energy for the Barrel. The square markers represent the photopeak efficiency normalized to the number of gamma rays emitted in the CALIFA Barrel geometrical acceptance, while the circles correspond to the total emitted gamma rays, independently of their direction.

acceptance effects, while the second is corrected by the geometrical acceptance of the Barrel. In both cases the algorithm uses a optimized angular window to cope with multiplicities larger than one.

The evaluation of where the undetected energy has been stopped is very important to improve the calorimeter design. Part of the Compton scattered or the backscattering gamma rays could escape the detector through the backward angles aperture, not covered by crystals. Another part, mainly at the highest energies, could escape after passing through the detector Barrel crystals. A specific simulation for testing where the energy escapes has been performed, measuring the number of detections and the energy spectra (i) in the crystals, (ii) in the backward region not covered by the crystals, (iii) around the Barrel section and (iv) in the passive material (the wrapping and carbon fibre alveoli).

To perform a realistic evaluation, the simulation considers gamma rays emitted at different energies in the projectile frame and, therefore, the energies at the Barrel vary with the polar angle. The angular range of the emitted particles have been constrained to the geometrical aperture of the Barrel section. Fig. 9 shows the energy spectra emitted and absorbed in the calorimeter elements, when gamma rays of 1 MeV (upper pad) and 10 MeV (lower pad) in the projectile frame are emitted, again boosted at a velocity $\beta=0.82$. The energy spectra correspond to detection of gamma rays at laboratory energies and, therefore, the spectra are

influenced by the kinematics of the Lorentz boost; this result is evident in the emitted gamma rays spectrum (line a), with a flat energy distribution ranging from around 0.7 to 1.8 times the projectile frame energy. Immediately below, the next histogram (line b) corresponds to the energy spectrum in the crystals, that is, the detected energy. Below, in lines c and e, the energy which escapes beyond the Barrel outer surface and through backward

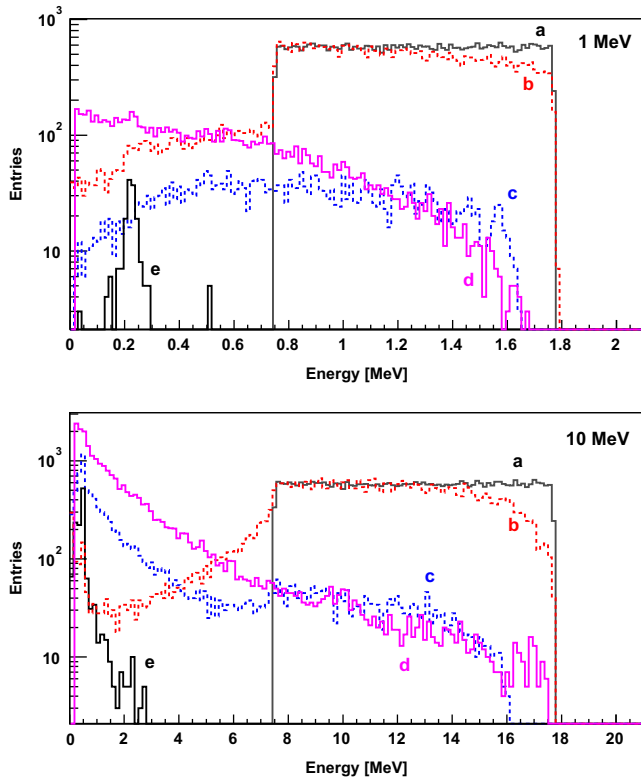


Fig. 9. Upper pad: energy spectra in the different regions and escaping zones for emitted gamma rays of 1 MeV in projectile frame. The line labeled a corresponds to the emitted energy spectrum, line b is the sum energy spectrum in the crystals and below, lines c and e correspond to the energy which escape beyond the Barrel outer surface and through the backward angle aperture, respectively. Line d corresponds to the energy spectrum absorbed by the passive matter. Lower pad: energy spectra in the different regions and escaping zones for emitted gamma rays of 10 MeV in projectile frame. Labels are equivalent to those of the top pad.

angle aperture are displayed, respectively. The last histogram, line d, corresponds to the energy spectrum which is not detected in any of the previous elements, that is, the energy absorbed by the inactive matter between the emission point and the end of the gamma ray life.

A more comprehensive evaluation at different energies can be done using Table 2, which contains the percentage of multiplicity one events (upper table) and the percentage of the total energy (lower table) deposited in the CALIFA crystals, the passive matter, dispersed in the backwards angle aperture and traversing through the crystals to escape behind the Barrel volume. The percentage of events with energy deposited in the crystal is divided into two parts: interaction in the Barrel crystals and a small contribution of interaction in the EndCap crystals, arising from scattered gamma rays, despite the fact that the angular range of the emitted particles have been selected to lie in the geometrical aperture of the Barrel section. Note that the percentage of events sums more than 100% due to the possibility of losing part of the energy in two or more different elements.

The percentage of energy (lower table in Table 2) is calculated from the integral of each energy spectra, normalized to the total energy emitted. The sum of the contributions in the different elements is 100%, once the escape through the forward beam pipe hole, in the order of 0.3%, is computed.

In the backward region (line e in Fig. 9), the spectrum is dominated by the Compton (at low emission energies) and $e^+ - e^-$ annihilation gamma rays (at high emission energies), with the 511 keV peak visible in the left side of the spectrum. Only a small fraction (below 4% even at the higher energies) of the gamma rays lost part of their energy in this region, with a total energy percentage of less than 0.1%. Escaping outside the Barrel section (line c), the energy spectrum spreads till the higher energies. The cases with some energy lost after crossing the Barrel account from 0.4% at 0.2 MeV to 30% of the total gamma rays at 15 MeV, but the energy portion escaping is in the order of 7% or below.

The passive matter considered in this simulation includes the crystals wrapping and the carbon fibre alveoli supporting the crystals. The number of gamma rays depositing part of the total energy in this passive material could be obtained from the analysis of Fig. 10, which represents the detected fraction of the emitted energy in two different media: in the calorimeter crystals alone (dashed histogram) or in a combination of the crystals, the space behind them and the space above the maximum angular coverage of 140.3° (the filled histogram). The upper pad displays the normalized multiplicity one events for

Table 2
Percentage of multiplicity one events (upper table) and of the emitted energy (lower table) deposited in the CALIFA crystals, in the passive matter, escaping after passing through the Barrel region and escaping through the backwards angles aperture. The energy in the first column corresponds to the emitted projectile frame gamma ray energies. See the text for further explanation.

Energy (MeV)	Crystals (Barrel + EndCap) (%)	Passive matter (%)	Barrel outer surface (%)	Backwards angle aperture (%)
Percentage of events with energy deposited in (or escaping through)				
0.2	99.2+1.2	7.4	0.4	0.3
0.5	98.6+3.0	12.0	2.2	0.4
1	96.5+4.0	15.3	7.6	0.4
2	93.7+5.4	23.1	14.6	0.7
5	92.9+9.7	34.1	18.7	1.7
10	94.8+16.3	50.9	23.4	3.0
15	96.1+21.3	63.7	30.0	3.9
Percentage of energy deposited in (or escaping through)				
0.2	97.1	2.3	0.4	0.1
0.5	93.9	4.0	1.8	0.1
1	88.6	6.0	5.0	0.1
2	83.6	8.2	7.7	0.1
5	84.0	8.0	7.6	0.1
10	84.4	8.5	6.5	0.1
15	85.6	8.0	6.0	0.1

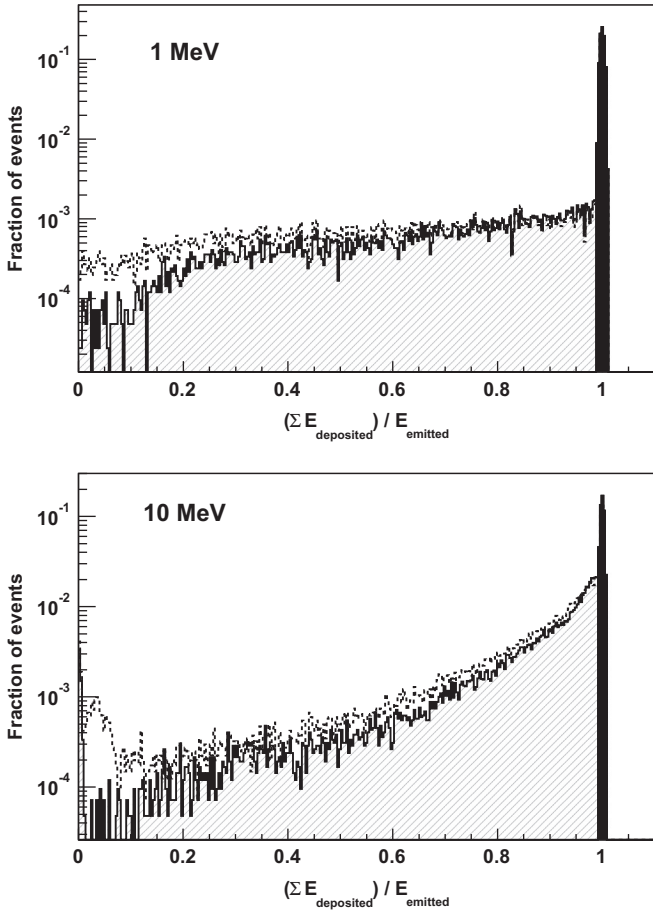


Fig. 10. Upper pad: fraction of multiplicity one events depositing energy in the calorimeter crystals (dashed histogram) and in the crystals and the escaping surfaces (patterned area and filled peak for the full reconstructed events), for emitted gamma rays of 1 MeV in projectile frame. The integral of the patterned area corresponds to the events with energy lost in the passive matter. The abscissa represents the ratio of the deposited energy to the emitted laboratory energies. Lower pad: same ratio for emitted gamma rays of 10 MeV in projectile frame. See the text for further explanation.

emitted gamma rays of 1 MeV (PF), while the lower pad for 10 MeV (PF). As the abscissa represents the ratio of the detected energy to the emitted laboratory energies, the full reconstructed gamma rays correspond to the peak shown in solid black. From the integral of the patterned and filled histograms, it is possible to obtain the percentage of gamma rays with some energy lost in the passive matter, as quoted in the third column of Table 2 (upper). The total energy lost in the passive material could be obtained from the integral of its energy spectrum, shown as line d in Fig 9, and specified in the third column of Table 2 (lower). The impressively low amount of energy deposited in the passive matter confirms the minimum incidence of the support structures and crystal wrapping in the gamma ray detection, despite the high granularity of the detector.

CALIFA should also work in many experiments as an efficient calorimeter, obtaining the individual energy for each emitted gamma ray in events with multiplicity above one. To check the efficiency of the CALIFA complete calorimeter under these conditions, several gamma rays of a given energy have been simultaneously emitted isotropically within the Barrel geometrical aperture. The reconstruction algorithm works to obtain the individual gamma rays, and their energy is summed to get the calorimetric properties of the detector.

An example of the outcome of this procedure, for multiplicity three, is shown in the upper pad of Fig. 11, where the peak at 3 MeV corresponds to the complete reconstruction and the sum of the energies of three gamma rays of 1 MeV each one, while the

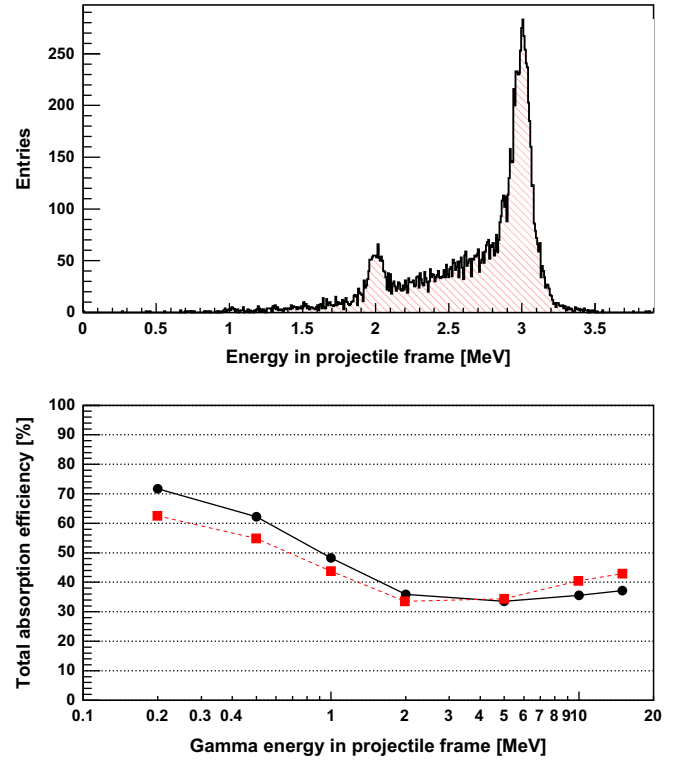


Fig. 11. Upper pad: energy spectrum of the reconstructed events with multiplicity three (that is, three gamma rays emitted with 1 MeV each one) in the Barrel. Lower pad: total absorption efficiency with respect to the emitted projectile frame gamma ray energy in events with multiplicity three in the Barrel acceptance (circles) or multiplicity five, with three gammas in the Barrel acceptance (squares). The energy of the peak where the efficiency is evaluated corresponds to three (five in the second case) times the energy in the abscissa.

small peak at 2 MeV represents events where only two gamma rays are reconstructed and the other does not deposit any energy. Other possibilities, such as the case that one of the particles is not completely reconstructed, or more than three clusters are found by the algorithm, return an incorrect sum energy, and therefore will contribute to the background as observed.

It is important to note that to obtain any calorimetric property it is mandatory to find the individual gamma ray energies and polar angles of each gamma ray emitted. Adding the energies deposited in the crystals without the proper identification of the individual gamma rays will not work due to the required transformation to the projectile frame, which requires both the energy and the angle.

The lower pad of Fig. 11 displays with circular symbols the total absorption efficiency in the reconstruction of the events of multiplicity three, where the three gamma rays are emitted with the same energy shown in the plot abscissa. The curve represents the efficiency results for the correct three-fold cluster detection with the proper sum energy. Note that for the typical spectroscopic energies below or around 1 MeV, the efficiency reconstructing the full cascade is quite high, close to 50%. In the same plot but marked with squares, the results when events with multiplicity five are considered, on condition that three of these gamma rays enter in the geometrical acceptance of the Barrel (as the previous case) while the other two are isotropically distributed and Doppler boosted (outside the Barrel geometrical acceptance). The gamma rays entering into the EndCap region are considered as fully detected. As before, the curve represents the efficiency when all the five gamma rays have been properly recorded and therefore the total energy is centred in the proper energy value, being the abscissa the projectile frame energy of each emitted gamma ray (and not the sum energy).

Note that the efficiency could be improved by identifying and adding the energy of separate clusters with 511 keV that are erroneously taken as an independent gamma ray emitted from the target region. This is even more important in the EndCap region where the energy, and so the cluster-fold, is larger than the Barrel region, as shown in Fig. 6. The present algorithm does not perform this correction, therefore underestimating the efficiency that the calorimeter could achieve.

5. Response to protons

We have calculated the total absorption efficiency of the CALIFA Barrel for monoenergetic protons emitted within the angular coverage of the Barrel. In fact, for the highest energies we have focused on the furthest forward angles as they are of particular importance for the planned study of (p,2p) reactions. Due to the particular kinematics of these reactions, in most of the cases we will have one proton in the direction of the forward EndCap and the other (with expected energies up to 320 MeV) directed towards the furthest forward rings of the Barrel.

With the aim of testing the performance of the Barrel in this situation we have generated monoenergetic protons of energies between 50 MeV and 200 MeV emitted isotropically within the angular acceptance of the Barrel, and monoenergetic protons of energies between 260 MeV and 320 MeV emitted in the most forward angles covered by the Barrel, i.e. between 43.5° and 48.5° . The energy deposited in the crystals has been collected and summed. The intrinsic scintillator energy resolution has been adjusted to 5% at 1 MeV, following the procedures described in Section 4.

In the top pad of Fig. 12, the energy spectrum for protons of 260 MeV is represented. The low energy tail of the peak is mainly due to the energy lost by the protons in the wrapping at the entrance window or between crystals. A correction has been applied to the spectrum by identifying events of crystal multiplicity two and three (the number of crystals fired) and adding an average energy loss due to the wrapping.

The bottom panel of Fig. 12 shows the total absorption efficiency of the Barrel for protons as a function of the energy. The two different curves correspond to the efficiency obtained according to two different criteria. The lower curve (circle symbols) represents the efficiency calculated by integrating the area below the total absorption peak within a window in the interval $[-2\sigma, 2\sigma]$. The upper curve (square symbols) represents the efficiency calculated by integrating the peak from the point at 90% of the nominal energy. The former definition applies more to spectroscopic applications in which the energy resolution is the most important parameter, whereas the latter applies more to calorimetric purposes in which the efficiency is the most important parameter and we just need to be sure that we have measured at least 90% of the energy of the incoming proton. In fact, an optimization of the algorithm correcting the proton energy according to the multiplicity would increase the efficiency defined by the former definition, leading to very similar results.

The high crystal granularity, necessary to correct for the Doppler effects in the gamma reconstruction, instigates problems in the detection of protons. The energy lost in the passive matter corresponding to the crystals wrapping cannot be recovered and the energy defect depends on the trajectory of the protons crossing the calorimeter and the number of traversed crystals (crystal-fold).

In order to determine the effect of the wrapping in the detection of protons, simulations have been performed with different prototype crystals of the Barrel detector [21]. The results from the simulation reproduces well the experimental results [12]. Analysis of the simulated events shows that the missing energy can be attributed to protons traversing the material between elements.

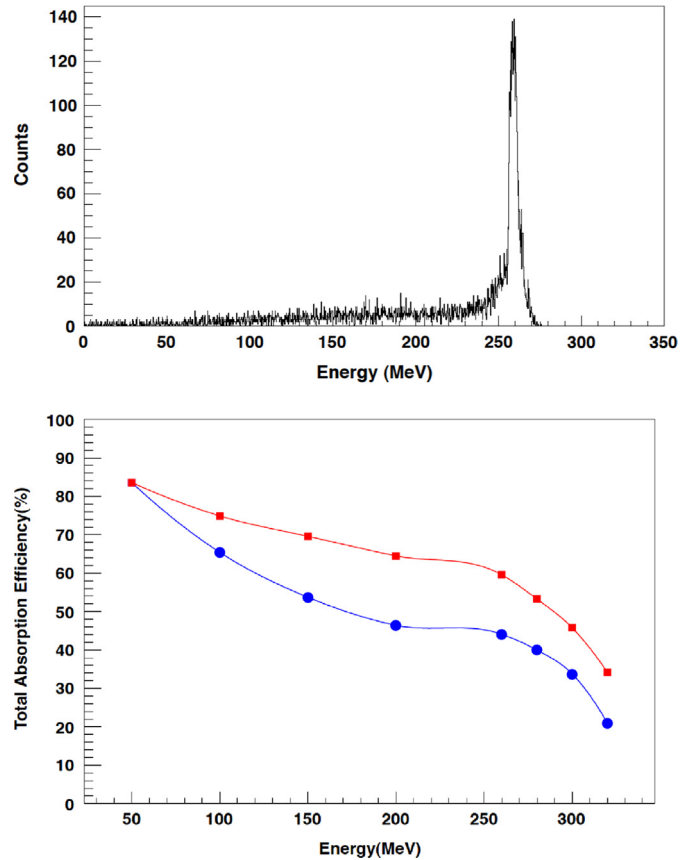


Fig. 12. Upper pad: energy spectrum of protons of 260 MeV corrected according to multiplicity (see text). Lower pad: total absorption efficiency for monoenergetic protons emitted within the angular coverage of the CALIFA Barrel, obtained integrating the area below the peak (two sigma criteria, lower curve with circle symbols) or integrating the area below the peak from 90% of the nominal energy (upper curve with square symbols).

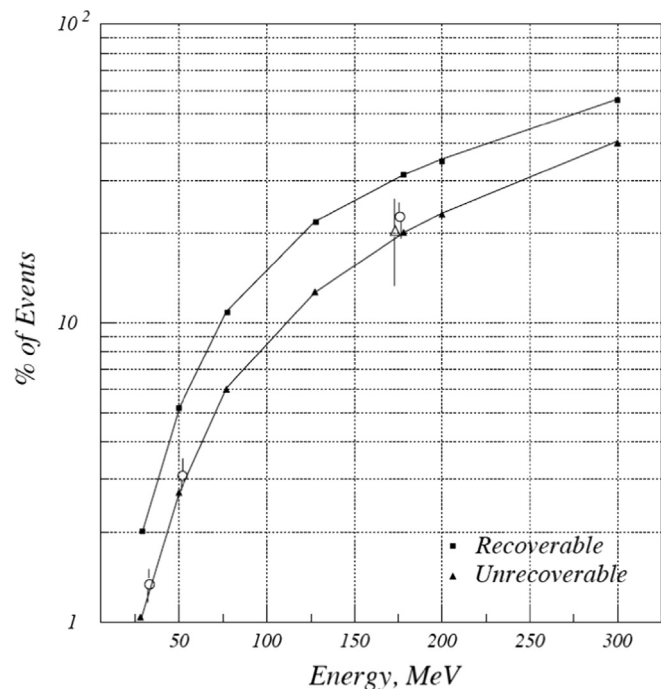


Fig. 13. Percentage of lost events which can be recovered by ideal add-back (filled squares) and those lost to inelastic process (filled triangles), calculated for a crystal of the CALIFA geometry. Data: open circles [22] and open triangles [21]. The line is drawn to guide the eye through calculated points. Taken from [21].

This effect was further confirmed by adding the energy lost in the foils to the energy deposited in the detector material. An important issue is also the maximum number of events that can be recovered using add-back. This number is limited by inelastic processes.

Fig. 13 shows the results of these calculations. The number of events lost due to inelastic processes was estimated from those falling outside of the full energy peak for an infinite detector block surrounding the target position. Subtracting the number of multiplicity one events that fall outside of the full energy peak for the central crystal in the simulated prototype from this number yields the ideal add-back factor. As an example, at an energy of 180 MeV the simulations predict that 21% of the events are lost to inelastic processes leading to a maximum full energy peak efficiency of 79%. Of these events 32% are recovered via add-back. The experimental value for irradiation through a single crystal is also given for comparison in the figure. One can note the excellent agreement between experiment and simulation. It was also deduced that an additional uncertainty of $\sim 7\%$ is due to protons scattering out of the back or front surfaces of the crystal. At low energies the fraction of inelastic events is small. However, at higher energies, e.g. 300 MeV, no protons deposit their full energy in a single crystal. In this case 60% of the events can be recovered via add-back.

6. Simulation of selected physical cases

We have evaluated the performance of the CALIFA Barrel under different physics scenarios. We have focused in two different cases of great interest for the R³B community where the CALIFA Barrel plays an important role: the spectroscopy of ²²O as an example of CALIFA acting as a high-resolution spectrometer and the ¹³²Sn deexcitation, where the decay of several dipole resonances is observed, as an example of CALIFA acting as an event calorimeter.

6.1. CALIFA as a high-resolution spectrometer

In this subsection the spectroscopy of ²²O is studied using a knockout reaction on ²³O, where CALIFA acts as a spectrometer detecting relatively low-energy gammas with low gamma ray multiplicity. This case exemplifies the performance of CALIFA as a high-resolution spectrometer.

The ²³O nucleus, with a neutron separation energy of 2.7 MeV, lies very close to the dripline and has no bound excited states below 4 MeV [23]. In the nuclide chart, it is surrounded by ²²O (A-1 core-fragment), with a first excited 2⁺ level at 3.17 MeV and ²⁴O (dripline) with no bound states [23]. Both neighbors seem to be double magic nuclei, indicating a persistence of the proton-magic number at Z=8 and (sub-)shell closures at N=14 and N=16. First experiments focusing on this nucleus yielded contradictory results concerning spin and parity assignment for the ground state of ²³O [24,25], which motivated a deeper investigation of this nucleus by using the neutron-knockout technique at relativistic energies (939 MeV/nucleon) at the FRS-GSI [26].

This experiment allowed the measurement of the core-fragment momentum distribution and gamma rays in coincidence, performed with a very basic array of 32 NaI(Tl).¹ Fig. 14 shows the energy spectrum of gamma rays recorded in coincidence with the ²²O fragments. This gamma ray spectrum was used to determine the exclusive cross-section for different final core-fragment states. The broad peak observed at higher energy is assumed to be due to the 3.1 MeV and the 2.6 MeV transitions that the NaI(Tl) detectors could not resolve. The exclusive momentum distributions were

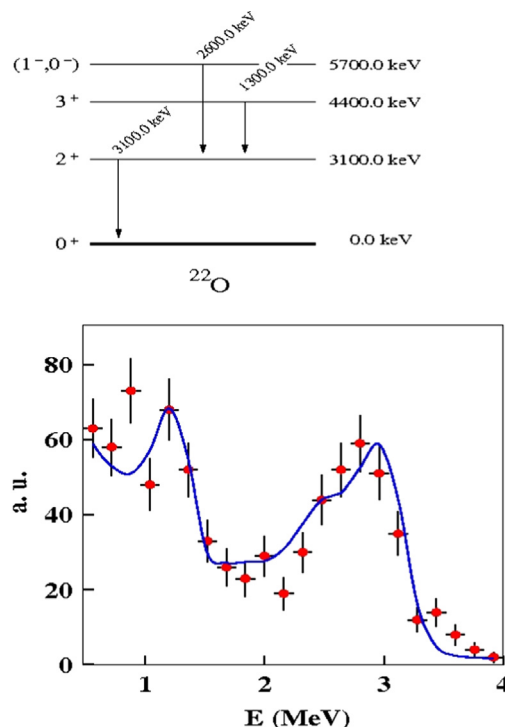


Fig. 14. Spectrum of gamma rays in coincidence with ²²O fragments after one-neutron removal from ²³O in a carbon target. The spectrum shown here has been obtained from the measured gamma ray spectrum after Doppler correction. The experimental spectrum (dots) is compared with the result of a GEANT3 simulation (line) adopting the level scheme shown above. Adapted from [26].

extracted assuming that all ²²O excited levels decay through the first excited state at 3.1 MeV. This peak was, therefore, used to gate the longitudinal momentum distribution in order to obtain the exclusive momentum distribution of the ²²O ground state that finally enabled a conclusion that the ground-state spin of ²³O is $I^\pi = 1/2^+$, which brought the experimental controversy to an end.

In order to demonstrate the resolution of the CALIFA Barrel in a spectroscopic experiment, the level scheme shown in Fig. 14 has been simulated in the CALIFA-R3BRoot code. The total number of entries has been selected to obtain a similar number to that of the experimental spectrum, while the population of the different levels has been adjusted to the experimental values. There is no attempt to reproduce any background or noise distribution over the simulated data; the experimental conditions were quite clear due to the time window which allow the separation of different contributions from the target interaction in the gamma ray detectors. The result of the simulation is shown in Fig. 15. The two gammas at 2.6 and 3.1 MeV are now perfectly separated, with energy resolutions of $\sim 5\%$ (5.6% and 4.7% from a Gaussian fit, respectively), while the peak at 1.3 MeV presents a resolution of $\sim 8\%$ (7.7% from the fit).

6.2. CALIFA as an event calorimeter

To demonstrate the calorimetric capabilities of CALIFA in a physics case with low gamma ray multiplicity per event we have used as an input for the simulation the GDR event generator (see Section 3.1) adapted to the ¹³²Sn case, where a high energy (16.1 MeV) GDR is combined with a lower energy (9.8 MeV) PDR, as it has been observed in experiments at the present LAND setup [27]. In Fig. 16 the simulated level scheme is presented.

The relative strengths of the PDR and the GDR Coulomb excitation cross-sections have been set to mimic the experimental results, but only photon decay was allowed. In addition a series of six discrete levels are included at lower energy. Their total

¹ Hexagons of 5 cm side and 20 cm thickness place 80 cm behind the knockout target in a wall configuration.

excitation probability (the probability of being populated as the first level) is 2.5% compared to the higher energy region. In this simulation the favorite decay channel of the giant and pygmy resonance is chosen to be the decay directly to the ground state, i.e. the probability to decay in a cascade via low-lying excited states is quite low compared to a single transition. The average multiplicity of the decay is thus low, with 60% of the events having multiplicity one. The probability of having an event with multiplicity two, three and four is 20%, 10% and 10%, respectively.

The excitation probability as produced in the event generator is shown in Fig. 17 (labeled simulation's input).

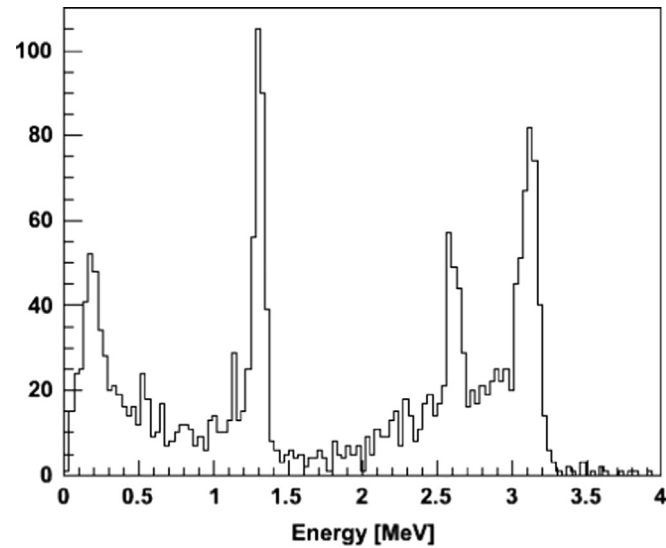


Fig. 15. Energy spectrum in CALIFA, after the analysis and Doppler correction of gammas emitted according to the level scheme shown in the previous figure. See the text for further explanation.

and PDR at 9.6 MeV are shown together with the discrete levels at lower energy. The events are generated according to this excitation probability.

The laboratory energies of the individual gamma rays in each event are reconstructed from the data collected by the calorimeter

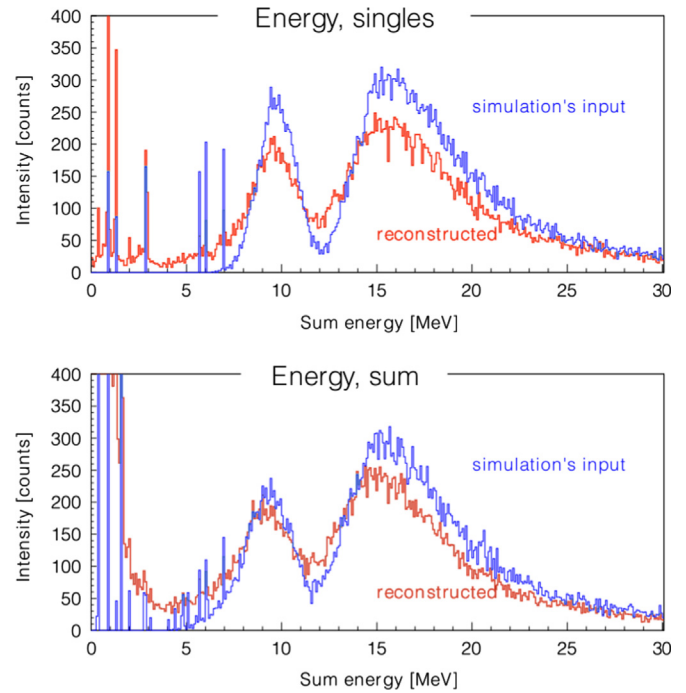


Fig. 17. Energy spectrum of the singles gamma rays (top) and sum energy per event (bottom). In both cases the spectrum used as an input for the simulation is shown together with the reconstructed one. The calorimetric sum spectrum is the total energy deposited in the calorimeter event by event.

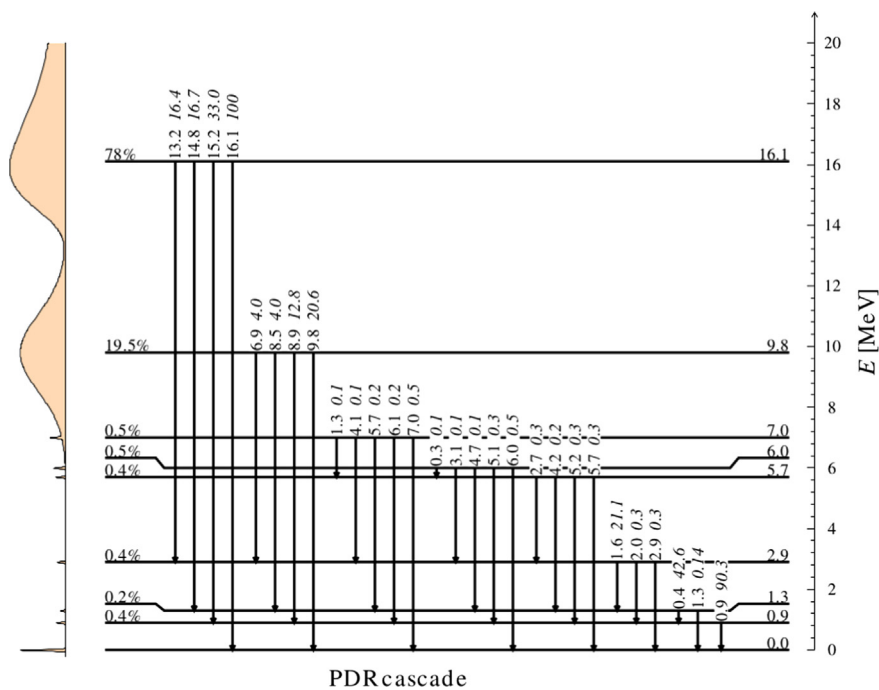


Fig. 16. Simulated level scheme for the pygmy dipole resonance physics case. The giant resonance at 16.1 MeV is combined with a pygmy resonance at 9.6 MeV, following the case of ^{132}Sn [27]. Only photon decays were allowed, i.e. no particles were emitted in the decay. The preferred decay channel is from the GDR directly to the ground state, which produces events with only one high-energy gamma ray emitted. The decay from the first excited state, fed from the higher levels, to the ground state produces a strong low energy transition in relation to multiplicity two or three events.

and transformed separately to the projectile frame, moving at a velocity $\beta=0.82$. In order to exclude the effect of the EndCap from the performances of CALIFA's barrel, the gamma rays emitted in its direction are analyzed without experimental uncertainties, i.e. they are ideally reconstructed. In 86% of the events the barrel contributed to the detection of the emitted gamma rays and only these events were taken into account in the analysis. In the analysis the clustering algorithm as described in Section 3.2 is used to determine photon energy and angle in order to perform the proper Doppler correction. The reconstructed photon energies are summed for every event, to determine the total excitation energy. The result is presented in Fig. 17 (labeled reconstructed). The difference between the input spectrum and the reconstructed one thus illustrates the detector response of CALIFA for this particular case.

In the reconstructed spectrum the PDR and GDR are reproduced and well separated. The distortion compared to the original input is mainly due to two effects: (i) due to their high energy, the gamma rays can escape the calorimeter without depositing their whole energy and (ii) in case of multiplicity higher than one, one of the gamma rays can escape the calorimeter. However, the realistic reproduction of the original features of the input distribution shows the excellent capabilities of CALIFA to act as a calorimeter in PDR studies.

The current case demonstrates the capabilities of CALIFA as a gamma ray spectrometer and as a calorimeter, providing excellent results in its performance.

7. Summary and conclusions

This evaluation of the performance of the CALIFA Barrel allows the assessment of the main features of the calorimeter, including its energy resolution, efficiency, passive vs. active matter balance and high multiplicity reconstruction capabilities. These characteristics were evaluated systematically over a broad energy and angular emission range, for the species that the calorimeter is sensitive to, namely gamma rays and protons, and also for key physical cases of interest for the R³B collaboration. The evaluation constitutes an accurate estimate of the final capabilities of the CALIFA Barrel before its construction and justifies the selected design, confirming that it achieves the required capabilities. It also aids in the design of ancillary and complementary detectors for the setup.

A set of computing tools have been developed for the evaluation: the R3BRoot program has been developed containing the simulation and evaluation components, including the complete CALIFA geometrical and physical response description, a set of event generators, methods for event reconstruction and analysis macros. Particular effort must be paid to the reconstruction with add-back, when data comes from several crystals, as a result of the high crystal multiplicity design for constraining Doppler broadening effects.

The evaluation of the Barrel efficiency and resolution in gamma rays offers a high commendation of the detector capabilities. The efficiency runs from close to 80% at low energies to 40% at 15 MeV while the resolution is limited by the scintillator intrinsic resolution at low energies and by the difficulties recovering all the energy from several crystals and the add-back procedure. The high value of the efficiency reflects the careful design, where passive matter is reduced to a minimum. This allows an efficient reconstruction of high multiplicity events, mandatory to the use of CALIFA for calorimetric purposes. The detection of high energy protons has been also studied, the efficiency found to be limited by inelastic processes at the highest energies expected for their angular coverage.

Finally, the study of some physical cases relevant for the R³B program have demonstrated the excellent characteristics of the CALIFA Barrel working as a high-resolution spectrometer and as an

event calorimeter in the particular experimental conditions envisaged for the detector.

Acknowledgments

This work was supported by the Spanish MICCIN FPA2009-14604-C02-01, the European Union Seventh Framework Programme FP7/2007-2013 under Grant agreement 262010 – ENSAR, the Portuguese FCT, Project PTDC/FIS/103902/2008 and by the Alliance Program of the Helmholtz Association (HA216/EMMI). The authors would like to acknowledge the R³B collaboration members for many discussions and valuable comments.

References

- [1] The FAIR Collaboration, FAIR CDR: An International Accelerator Facility for Beams of Ions and Antiprotons, Conceptual Design Report, Technical Report, GSI, 2001.
- [2] G. Muenzenberg, H. Geissel, *Journal of Physics Conference Series* 413 (2013) 012006. Proceedings of the International Summer School for Advanced Studies Dynamics of Open Nuclear Systems (PREDEAL12).
- [3] T. Aumann, B. Jonson, et al., Technical Proposal for the Design, Construction, Commissioning and Operation of R3B, A Universal Setup for Kinematical Complete Measurements of Reactions with Relativistic Radioactive Beams, 2005.
- [4] M. Gascón, H. Alvarez-Pol, J. Benlliure, E. Casarejos, D. Cortina-Gil, I. Durán, *IEEE Transactions on Nuclear Science* NS-55 (2008) 1259.
- [5] H. Alvarez-Pol, J. Benlliure, E. Casarejos, D. Cortina, I. Durán, M. Gascón, *Nuclear Instruments and Methods in Physics Research B* 266 (2008) 4616.
- [6] The CALIFA Collaboration, CALIFA Barrel Technical Design Report, 2012, Approved January 2013.
- [7] E. Casarejos, H. Alvarez-Pol, D. Cortina-Gil, I. Durán, P. Izquierdo, P. Yañez, J.A. Vilán, The mechanical design of the BARREL section of the detector CALIFA for R3B-FAIR. EPJ Web of Conferences, vol. 66, 2014 INPC 2013 – International Nuclear Physics Conference, Firenze, Italy, June 2–7, 2013, <http://dx.doi.org/10.1051/epjconf/20146611037>.
- [8] M. Gascón, H. Alvarez-Pol, S. Ancelin, J. Benlliure, E. Casarejos, D. Cortina-Gil, I. Durán, M. Josselin, J.A. Scarpaci, J. Peyré, *IEEE Transactions on Nuclear Science* NS-56 (2009) 962.
- [9] M. Gascón, H. Alvarez-Pol, J. Benlliure, E. Casarejos, D. Cortina-Gil, I. Durán, D. González, N. Montes, *IEEE Transactions on Nuclear Science* NS-57 (2010) 1465.
- [10] M. Gascón, Prototype of a new calorimeter for the studies of nuclear reactions with relativistic radioactive beams (Ph.D. thesis), Universidade de Santiago de Compostela, 2010.
- [11] M. Bendel, R. Gernhäuser, W.F. Henning, R. Krücken, T. Le Bleis, M. Winkel, *The European Physical Journal A* (2013) 49.
- [12] B. Pietras, M. Gascón, H. Alvarez-Pol, M. Bendel, T. Bloch, E. Casarejos, D. Cortina-Gil, I. Durán, E. Fiori, R. Gernhäuser, D. González, T. Kröll, T. LeBleis, N. Montes, E. Nacher, M. Robles, A. Perea, J.A. Vilán, M. Winkel, *Nuclear Instruments and Methods in Physics Research A* 729 (2013) 77.
- [13] D. Bertini, *Journal of Physics: Conference Series* 331 (2011) 032036.
- [14] H. Alvarez-Pol, M. Al-Turany, D. Bertini, D. Kresan, GSI Scientific Report 2012, GSI-SR2012-IMPRINT, PHN-ENNA-EXP-71, 205.
- [15] D. Bertini, M. Al-Turany, I. Koenig, F. Uhlig, *Journal of Physics: Conference Series* 119–3 (2008) 032011.
- [16] Rene Brun, Fons Rademakers, in: Proceedings AIHENP'96 Workshop, Lausanne, September 1996. *Nuclear Instruments and Methods in Physics Research A* 389 (1997) 81–86. See also (<http://root.cern.ch/>).
- [17] S. Agostinelli, J. Allison, K. Amako, J. Apostolakis, H. Araujo, P. Arce, M. Asai, D. Axen, S. Banerjee, G. Barrand, F. Behner, L. Bellagamba, J. Boudreau, L. Broglia, A. Brunengo, H. Burkhardt, S. Chauvie, J. Chuma, R. Chytráček, G. Cooperman, G. Cosmo, P. Degtyarenko, A. Dell'Acqua, G. Depaola, D. Dietrich, R. Enami, A. Feliciello, C. Ferguson, H. Fesefeldt, G. Folger, F. Foppiano, A. Forti, S. Garelli, S. Giani, R. Giannitrapani, D. Gibin, J.J. Gomez Cadenas, I. Gonzalez, G. Gracia Abril, G. Greeniaus, W. Greiner, V. Grichine, A. Grossheim, S. Guatelli, P. Gumplinger, R. Hamatsu, K. Hashimoto, H. Hasui, A. Heikkinen, A. Howard, V. Ivanchenko, A. Johnson, F.W. Jones, J. Kallenbach, N. Kanaya, M. Kawabata, Y. Kawabata, M. Kawaguti, S. Kelner, P. Kent, A. Kimura, T. Kodama, R. Kokoulin, M. Kossov, H. Kurashige, E. Lamanna, T. Lampn, V. Lara, V. Lefebvre, F. Lei, M. Liendl, W. Lockman, F. Longo, S. Magni, M. Maire, E. Medernach, K. Minamimoto, P. Mora de Freitas, Y. Morita, K. Murakami, M. Nagamatsu, R. Nartallo, P. Nieminen, T. Nishimura, K. Ohtsubo, M. Okamura, S. O'Neale, Y. Oohata, K. Paech, J. Perl, A. Pfeiffer, M.G. Pia, F. Ranjard, A. Rybin, S. Sadilov, E.D. Salvo, G. Santin, T. Sasaki, N. Savvas, Y. Sawada, S. Scherer, S. Sei, V. Sirotenko, D. Smith, N. Starkov, H. Stoecker, J. Sulkimo, M. Takahata, S. Tanaka, E. Tcherniaev, E.S. Tehrani, M. Tropeano, P. Truscott, H. Uno, L. Urban, P. Urban, M. Verderi, A. Walkden, W. Wander, H. Weber, J.P. Wellisch, T. Wenaus, D.C. Williams, D. Wright, T. Yamada, H. Yoshida,

- D. Zschiesche, Nuclear Instruments and Methods in Physics Research Section A 506 (2003) 250.
- [18] A.S. Goldhaber, Physics Letters B 53 (1974) 306.
- [19] E. Yoshida, K. Shizuma, S. Endo, T. Oka, Nuclear Instruments and Methods in Physics Research Section A 484 (2002) 557.
- [20] P. Teubig, Development of reconstruction algorithms for CALIFA (Ph.D. thesis program), Universidade de Lisboa, 2012.
- [21] D.D. DiJulio, V. Avdeichikov, J. Cederkall, P. Golubev, B. Jakobsson, H. Johansson, C. Tintori, Nuclear Instruments and Methods in Physics Research Section A 612 (2009) 127.
- [22] V. Avdeichikov, A.S. Fomichev, B. Jakobsson, A.M. Rodin, G.M. Ter-Akopian, Nuclear Instruments and Methods in Physics Research Section A 439 (2000) 158.
- [23] M. Stanoiu, F. Azaiez, Z. Dombri, O. Sorlin, B.A. Brown, M. Belleguic, D. Sohler, M.G. Saint Laurent, M.J. Lopez-Jimenez, Y.E. Penionzhkevich, G. Sletten, N.L. Achouri, J.C. Anglique, F. Becker, C. Borcea, C. Bourgeois, A. Bracco, J.M. Daugas, Z. Dlouhy, C. Donzaud, J. Duprat, Z. Fulp, D. Guillemaud-Mueller, S. Grvy, F. Ibrahim, A. Kerek, A. Krasznahorkay, Physical Review C 69 (3) (2004) 034312.
- [24] E. Sauvan, F. Carstoiu, N.A. Orr, J.C. Anglique, W.N. Catford, N.M. Clarke, M. Mac Cormick, N. Curtis, M. Freer, S. Grvy, C.L. Brun, M. Lewitowicz, E. Ligard, F.M. Marqus, P. Roussel-Chomaz, M.G.S. Laurent, M. Shawcross, J.S. Winfield, Physics Letters B 491 (1–2) (2000) 1.
- [25] R. Kanungo, M. Chiba, N. Iwasa, S. Nishimura, A. Ozawa, C. Samanta, T. Suda, T. Suzuki, T. Yamaguchi, T. Zheng, I. Tanihata, Physical Review Letters 88 (2002) 142502.
- [26] D. Cortina-Gil, J. Fernandez-Vazquez, T. Aumann, T. Baumann, J. Benlliure, M.J.G. Borge, L.V. Chulkov, U. Datta Pramanik, C. Forssn, L.M. Fraile, H. Geissel, J. Gerl, F. Hammache, K. Itahashi, R. Janik, B. Jonson, S. Mandal, K. Markenroth, M. Meister, M. Mocko, G. Munzenberg, T. Ohtsubo, A. Ozawa, Y. Prezado, V. Pribora, K. Riisager, H. Scheit, R. Schneider, G. Schrieder, H. Simon, B. Sitar, A. Stolz, P. Strmen, K. Summerer, I. Szarka, H. Weick, Physical Review Letters 93 (2004) 062501.
- [27] P. Adrich, A. Klimkiewicz, M. Fallot, K. Boretzky, T. Aumann, D. Cortina-Gil, U.D. Pramanik, T.W. Elze, H. Emling, H. Geissel, M. Hellstrm, K.L. Jones, J.V. Kratz, R. Kulesa, Y. Leifels, C. Nociforo, R. Palit, H. Simon, G. Surwka, K. Summerer, W. Walus, Physical Review Letters 95 (2005) 132501.